Chemical Physics 422 (2013) 175–183

Contents lists available at SciVerse ScienceDirect

Chemical Physics

journal homepage: www.elsevier.com/locate/chemphys

Theoretical examination of picosecond phenol migration dynamics in phenylacetylene solution

Lucas Kocia [a,b], Steve M. Young [a,*], Yana A. Kholod [c,d], Michael D. Fayer [e], Mark S. Gordon [c], Andrew M. Rappe [a]

[a] Makineni Theoretical Laboratories, Department of Chemistry, Philadelphia, PA 19104-6323, United States
[b] Department of Chemistry, Harvard University, Cambridge, MA 02138, United States
[c] Ames Laboratory of US DOE and Department of Chemistry, Iowa State University, Ames, IA 50011, United States
[d] Department of Chemistry, Medical Technology and Physics, Monmouth University, West Long Branch, NJ 07764, United States
[e] Department of Chemistry, Stanford University, Stanford, CA 94305-5080, United States

ARTICLE INFO

Article history:
Available online 1 May 2013

Keywords:
Molecular dynamics
ab initio
Vibrational echo
Hydrogen bonding

ABSTRACT

The time-dependent dynamics of phenol dissolved in liquid phenylacetylene is theoretically investigated through first-principles calculations and molecular dynamics. By modeling the hydroxyl functional group with a Morse potential, the bond becomes site-sensitive, vibrating at distinct frequencies when bound at the phenylacetylene triple bond and aromatic ring. This can be exploited to simulate 2D-IR echo spectra using Fourier analysis. The resulting dynamics yields a phenol migration time between the two primary binding sites on phenylacetylene of 3–5 ps in excellent agreement with experiment. Furthermore, this study finds that the mechanism for this migration is strongly influenced by an indirect pathway, in contrast to prior experimental interpretation. The dynamics is found to be primarily dictated by van der Waals forces instead of hydrogen bonding forces, a conclusion that is supported by first principles calculations.

1. Introduction

The dynamics of liquids remains one of the larger unsolved problems in theoretical chemistry. Understanding liquid motions and ordering is crucial to solving problems ranging from effective *in situ* drug delivery [1] to electrochemical cell design [2]. In particular, the dynamics of electrostatic interactions between electrophiles and conjugated aromatic molecules is poorly understood [3]. Such interactions occur commonly in organic liquids, for instance, in solvent interactions and during many self-assembly processes [4]. Of special importance are species capable of hydrogen bonding [5–7]. The presence of hydrogen bonding can dominate liquid dynamics; the most prominent example is water, which has been extensively studied, both experimentally and theoretically [8–17].

Recently, systems featuring hydrogen-π bonding have attracted great interest. A particularly interesting case is phenol dissolved in phenylacetylene. The presence of both an aromatic ring and a carbon–carbon triple bond (hereafter referred to as the "ring" site and the "triple" site respectively) provide two distinct hydrogen-π binding options for the hydroxyl group hydrogen of phenol [18–22]. Though differing in energetic favorability, they are similar enough to compete in equilibrium. As a result, phenol exhibits migratory behavior between these sites when in solution with phenylacetylene.

This behavior has been investigated using two-dimensional infrared (2D-IR) vibrational echo spectroscopy. Briefly, an initial pair of light pulses creates a population of vibrationally excited molecules. After a defined waiting period, a third pulse induces an emission from these excited states that is observed as an echo [23–26]. The frequency of the absorbed radiation can be plotted against that of the emitted radiation; an off-diagonal peak indicates a change in environment during the waiting period, such as a transition between hydrogen bonding at different sites [27,28]. In a solution of 0.1 M phenol dissolved in phenylacetylene, distinct hydroxyl stretch frequencies associated with the free (unbound) state, hydrogen bonding at the ring site, and hydrogen bonding at the triple site were observed [18]. From the rate of growth of off-diagonal peaks upon the application of three pulses to stimulate a vibrational echo, it was determined that the migration time of phenol between the triple and ring sites was ≈ 5 ps [18].

Though this experimental technique can determine the rate of phenol migration between two phenylacetylene hydrogen binding sites, the experiment cannot reveal the mechanism for this process. *a priori*, possible mechanisms include migration of a phenol

* Corresponding author.
E-mail address: smyoung@sas.upenn.edu (S.M. Young).

0301-0104/$ - see front matter © 2013 Elsevier B.V. All rights reserved.
http://dx.doi.org/10.1016/j.chemphys.2013.04.015

terminal hydroxyl group along the backbone of an adjacent phenylacetylene (a "direct" migration), and intermolecular hopping from one site to another, possibly with a free intermediate state (an "indirect" migration). The role of indirect migrations was examined experimentally by taking the 2D-IR spectra of solutions diluted with carbon tetrachloride. The additional carbon tetrachloride reduces the likelihood of indirect migration because it becomes more difficult for a phenol to encounter two adjacent phenylacetylenes. Since this dilution had no significant effect on the growth of the off-diagonal peaks, it was tentatively concluded that direct migration of a bonded phenol molecule between sites of one phenylacetylene is the primary mechanism of exchange [18].

In this work, the dynamics of phenol migration in phenylacetylene was investigated using quantum chemistry calculations and classical molecular dynamics (MD) with potentials that were carefully fitted to *ab initio* data. In addition to reproducing the 2D-IR spectra of the experimental study, further analysis reveals mechanistic details that are inaccessible to experiment, giving new insights into how molecules associate and move in liquids. In particular, it was found that indirect migrations are actually slightly favored over direct migrations, although both occur, and that the experimental assumption that indirect migration proceeds via a second-order reaction rate, while direct migration follows a first-order reaction rate, is likely incorrect.

2. Computational approach

Using the electronic structure code GAMESS[29], the Effective Fragment Potential (EFP) method[30] and second order Møller-Plesset perturbation theory (MP2) were used to study phenol-phenylacetylene complexes. The EFP method is derived from first principles quantum mechanics and provides a computationally inexpensive and highly accurate alternative to standard *ab initio* quantum chemistry approaches, such as Hartree–Fock (HF) and Density Functional Theory (DFT). Single molecules are represented as rigid fragments, and the corresponding fragment-fragment interactions consist of the following energy terms: Coulomb, polarization/induction, exchange-repulsion, dispersion, and charge transfer interactions. The polarization term is iterated to self-consistency. All of these terms are derived from first principles quantum mechanics and contain no empirically fitted parameters. In previous studies of H-bonding [31] and π-π interactions[32], the ability of the EFP method to describe both kinds of interactions correctly was demonstrated. EFP potentials for phenol and phenylacetylene were used to determine minima for the phenol-phenylacetylene complex. Next, the *ab initio* MP2 method was used to refine the EFP structures. The interaction of phenol and phenylacetylene, as with most aromatics, is strongly dictated by weakly interacting van der Waals (vdW) forces [33]. We and others have found that MP2 handles long-range electron correlation effects very well[34–36]. Classical MD force fields were fitted to the final MP2 results for subsequent modeling of the system at longer length scales.

MD force fields were developed by modifying the Generalized Amber Force Field (GAFF)[37] values to produce binding site geometries and energies and migration barriers between sites that agree more closely with MP2 results. This included reparameterizing the phenol C-O-H harmonic angular force field and changing the phenol O-H harmonic bond force field to a Morse potential. The angular terms were fitted to *ab initio* MP2 results, while the Morse potential strength was fitted to reproduce the experimentally observed frequency [18]. These modifications imparted the necessary flexibility and accuracy to the hydroxyl, enabling it to undergo bonding and migration with phenylacetylene more realistically. Most notably, the designed classical molecule exhibits vibrational sensitivity when bound at different binding sites, as seen experimentally. All remaining force field terms involving bonds, angles, and dihedrals between the carbon and hydrogen atoms were left unmodified, and therefore harmonic in form with GAFF values.

This approach differs from that taken previously in the study of a similar benzene-phenol system[38]. In that work, all force fields were kept harmonic, and the phenol terminal C-O-H angle was fixed at 180°. Lacking vibrational site sensitivity at the terminal O-H bond, binding events were determined using a linear response function, and dipole moments were obtained via the linear Stark effect to determine site-binding. The present work accomplishes this more naturally and more faithfully reproduces the experiment by using the site-dependent frequency shift in the O-H vibration of phenol during hydrogen bonding.

3. Methods

First, the ground states of isolated phenol and phenylacetylene molecules were located at the MP2/6-31G(d) level of theory. EFP potentials were generated for these structures using the 6-311++G (3df,2p) basis set. Then, several starting geometries were used to locate low-energy structures on the potential energy surface of the phenol-phenylacetylene dimer using Monte-Carlo sampling with simulated annealing (MC/SA) from 12000 K down to 100 K. The EFP fragments were put in a $20 \times 20 \times 20$ Å^3 periodic box. Local Newton–Raphson optimizations were performed after every 200 MC/SA steps. The geometries of the located low-energy structures were then optimized using the EFP method. All energy minima were confirmed to have only positive Hessian eigenvalues. The structures corresponding to EFP potential energy minima were then used as starting geometries to locate phenol-phenylacetylene complex minima at the MP2 level of theory with 6-31 + G(d,p) and 6-311++G(d,p) basis sets.

The MD simulations were performed on a system of 99 phenylacetylene molecules and 1 phenol molecule using the LAMMPS package [39]. Though effectively infinitely dilute, in the present context this system provides an environment equivalent to the 0.1 M phenol solution used for the 2D-IR measurements [18]. Further simulations were carried out on a system of 37 phenylacetylene molecules, 62 carbon tetrachloride molecules and 1 phenol molecule. This corresponds to the concentration reported in diluted samples containing a 0.60 mol ratio between phenylacetylene and carbon tetrachloride[18]. These systems were placed in a cubic box with periodic boundary conditions in an *NPT* ensemble. Nosé-Hoover[40] barostatting was used, with a damping time constant of 1 ps and thermostatting every 1 ps. Fifty initial molecular configurations were allowed to evolve under 1 atm and 300 K until the supercell volume oscillated around an equilibrium value.

After that, 1 ns runs were performed at 1 atm and 300 K producing 50 ns of total data. Coulombic forces were calculated using an Ewald summation. The charges used for phenol were $q_{C1} = -0.2e, q_{C2} = -0.078e, q_{C3} = -0.339e, q_{C4} = 0.368e, q_{H1} = 0.141e, q_{H2} = 0.144e, q_{H3} = 0.178e, q_{H4} = 0.381e$, and $q_O = -0.5e$, where the index number increases as the terminal hydroxyl is approached. The harmonic C-O-H angle parameters were $K = 55.0$ kcal/mol and θ = 109.0°. The terminal O-H Morse bond parameters were D = 100.0 kcal/mol, α = 1.68 Å and $r_0 = 0.966895$ Å. The charges used for phenylacetylene were $q_{C1} = -0.089e, q_{C2} = -0.051e, q_{C3} = -0.04e, q_{C4} = -0.01e, q_{C5} = -0.037e, q_{C6} = -0.19e, q_{H1} = 0.02e, q_{H2} = 0.088e, q_{H3} = 0.093e$, and $q_{H4} = 0.126e$, where the index number increases as the terminal acetylene is approached. The Lennard–Jones (LJ) parameters for phenol were $\epsilon_C = 0.11$ kcal/mol, $\sigma_C = 2.599643$ Å. Finally, the charges used for carbon tetrachloride were $q_C = -4e, q_{Cl} = 0.248e, \epsilon_C = 0.05$ kcal/mol, $\sigma_C = 3.8$ Å, $\epsilon_{Cl} =$

0.266 kcal/mol, $\sigma_{Cl} = 3.47$ Å and the CCl_4 angles were set to be rigid. The remaining bond, angle and dihedral force parameters were set to AMBER standard values.

4. *ab initio* Results and MD potential fitting

Ab initio calculations were performed both to characterize the bound states and interactions of phenol and phenylacetylene and to inform the construction of a classical potential for MD. First, the energy minima of the phenol-phenylacetylene complex were identified. EFP calculations were performed as an initial step, followed by MP2 calculations to refine the EFP energy minima. Fig. 1 shows the minima that were identified. The two lowest minima feature clear hydrogen bonding to the triple site of phenylacetylene. The other three minima feature hydrogen bonding with ring carbons and are approximately 1.0 kcal/mol higher in energy than the triple-site hydrogen binding configurations. In all cases, the phenol ring prefers to form stacking or near stacking geometries with the phenylacetylene ring, rather than T-like states where the long axis of phenol is perpendicular to that of phenylacetylene. This demonstrates the strength of the π–π stacking interaction and suggests that it plays an important role in solution dynamics. Given the significance of minimum energy configurations to the dynamics, these minima constituted the most important benchmarks for evaluating the MD potentials. The minima identified using the MD potentials agree very well with the *ab initio* results, in both geometry and energy, as seen in Fig. 1.

Since understanding the migration of phenol is a major objective of this study, our next benchmark consisted of minimum energy configurations at different positions along the length of phenylacetylene molecule. The oxygen of phenol was constrained to lie in a plane normal to the phenylacetylene backbone at regular intervals along it. These are shown in Fig. 2, along with the energy of the corresponding MD geometry found using the same procedure. As with the unconstrained minima, the MD potentials reproduce the *ab initio* results quite well.

For a more global assessment of the MD potential quality, two additional slices of the potential energy surface were considered. At various points along the phenylacetylene backbone the phenol was allowed to minimize a single coordinate: the distance of the phenol hydrogen to the plane of the phenylacetylene ring. This was done with the phenol ring both parallel and perpendicular to the phenylacetylene ring, referred to as "T-complex" and "stacking", respectively. In both cases, the individual molecule geometries were fixed to their respective minima. The results are shown in Fig. 3; for both orientations the MD energies and minimized intermolecular distances agree well with their *ab initio* counterparts.

Overall, the MD potentials conform excellently to the *ab initio* behavior of the phenol-phenylacetylene complex. Finally, the dipole moments of each molecule deviate minimally from their *ab initio* values, and the liquid densities obtained from MD are in reasonable agreement with experiment (Table 1).

5. Simulated IR and 2D-IR spectra and comparison to experiment

5.1. IR spectra

To confirm the validity of the MD potential, IR spectra were simulated from the MD trajectory data. The frequency of the anharmonic O-H bond in the phenol is sensitive to hydrogen bonding and this allows for the direct calculation of the IR spectrum from the dipole trajectory. This is equivalent to the corresponding experimental IR spectrum via the fluctuation–dissipation theorem. The absorption line shape function is,

$$I(\omega) = \left\langle \left| \Sigma_\alpha \int_{t_{min}}^{t_{max}} q_\alpha r_\alpha(t) e^{-i\omega t} dt \right|^2 \right\rangle$$

where $\langle \ldots \rangle$ denotes a signal average (in this case, over the 50 runs of the MD simulation) and q_α and $r_\alpha(t)$ are the charge and position of the α atom in the run at time t. The calculated IR spectrum from a 0.1 M MD simulation is shown in Fig. 4(c) and agrees extremely well with the experimental IR peaks in Fig. 4(a). Also shown in Figs. 4(d) and (b) are the corresponding spectra when the solution is diluted with carbon tetrachloride. These spectra exhibit good qualitative agreement. The quality of the calculated spectra is lower since the MD potential for carbon tetrachloride was not optimized for this system.

5.2. 2D-IR spectra

2D-IR spectra were constructed by splitting the trajectory into smaller time intervals, and Fourier transforming the dipole data to get an IR spectrum for each interval. This essentially provides

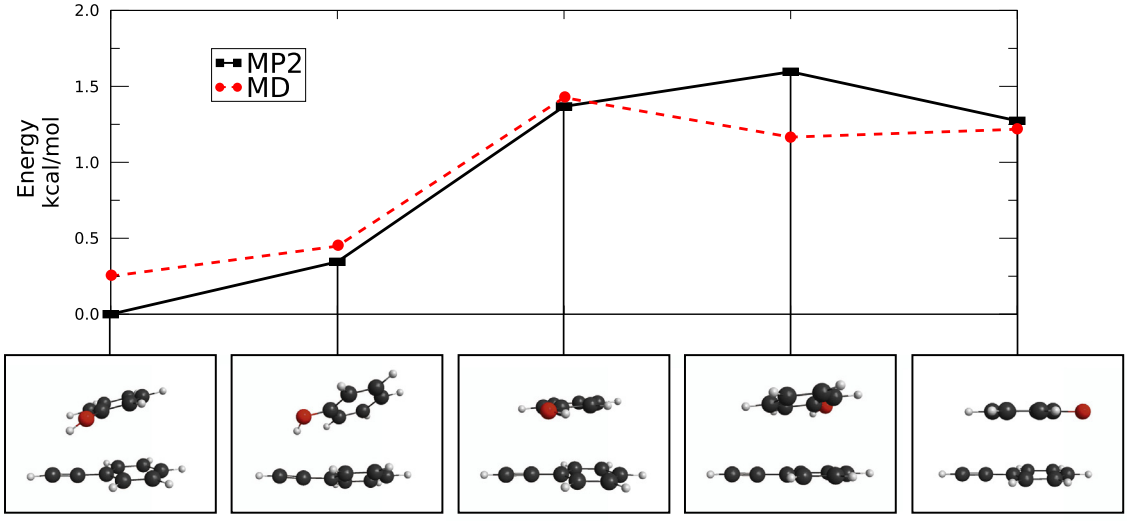

Fig. 1. The relative energies of phenol-phenylacetylene energy minima located with MP2/6–31G+(d,p) plotted against the corresponding minimum energies found using the MD potentials. The structure for each energy minimum is shown below the plot. The structures are dominated by the π-π stacking interaction of the aromatic rings on each molecule, with those permitting hydrogen bonding to the triple bond constituting the lowest energy structures.

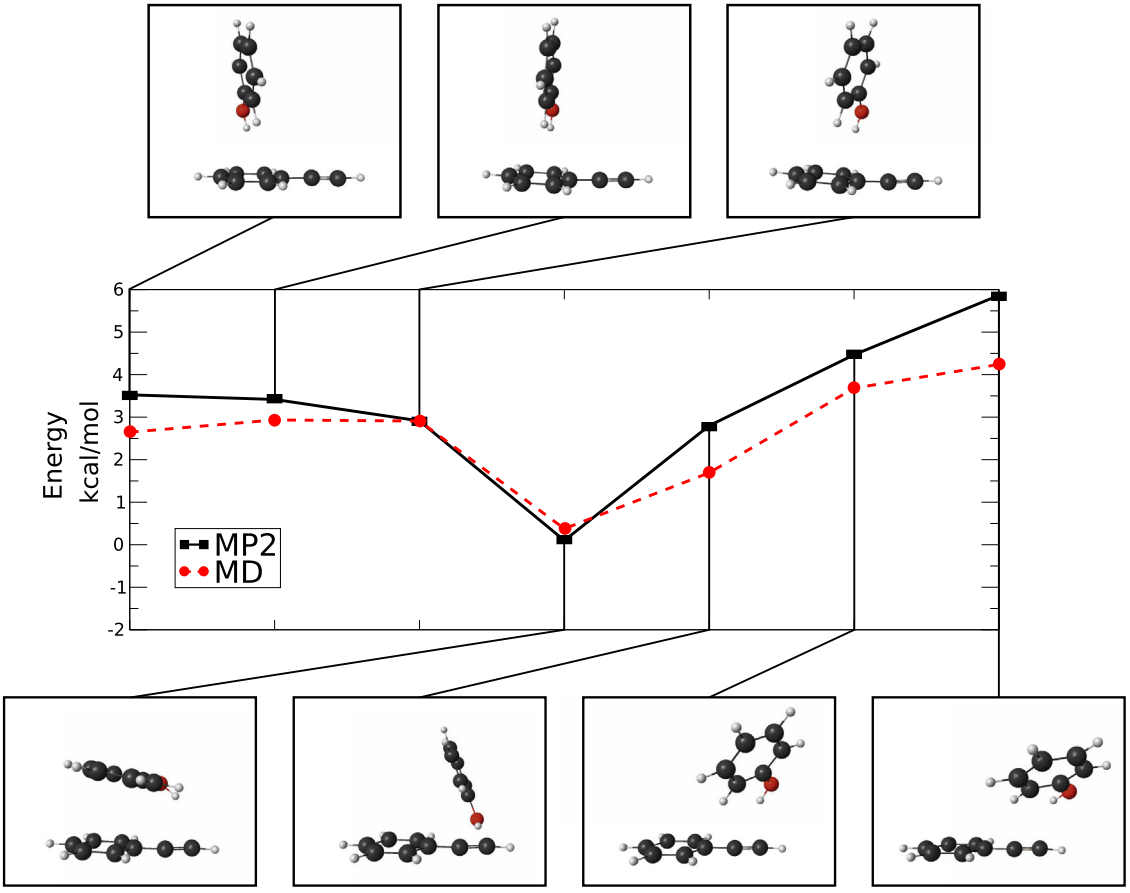

Fig. 2. Comparison between MD and MP2 energy minima obtained with the phenol oxygen constrained to lie a fixed distance along the backbone of phenylacetylene. The optimized structures corresponding to the plotted minima are above and below the graph and indicated by lines running from the data points. Both the preference for stacking behavior and the relative flatness of the potential energy surface are reinforced.

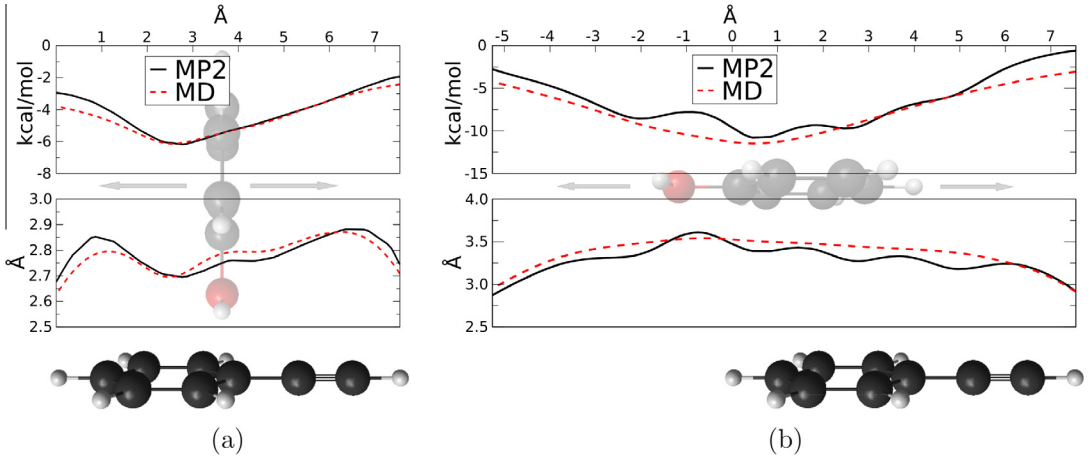

Fig. 3. Comparison between the MD and MP2 results for slices of the potential energy surface. The phenol and phenylacetylene geometries and orientation were fixed as either (a) T-complex, where the phenol ring is perpendicular to the phenylacetylene ring, or (b) stacking, where the phenol ring lies parallel to the phenylacetylene ring, while phenol was scanned along the backbone of phenylacetylene, with only the phenol-phenylacetylene distance allowed to relax. The horizontal axis gives the location of the phenol hydrogen along the phenylacetylene backbone underneath the plots. The top graphs show the energy of the complexes while the lower graph gives their phenol-phenylacetylene distance.

an intensity function $F(\omega,t)$ with time and frequency dependence. Then, for a given waiting period τ, one can find the 2D-IR intensity at (ω,ω') by computing $F(\omega,t)F(\omega,t+\tau)$ and integrating over time t. Due to the uncertainty relationships inherent in Fourier analysis, the finer the frequency grid, the larger the uncertainty in this delay. A window of 4 ps was found to provide the necessary frequency resolution while maintaining sufficient temporal precision.

Simulated 2D-IR spectra are displayed in Fig. 5. These graphs have off-diagonal peaks that grow in by 3–5 ps, consistent with

Table 1
A comparison of the equilibrium (T = 300 K, P = 1 atm) liquid density, and single-molecule charge and dipole moments of experimental, *ab initio* and MD phenol and phenylacetylene.

Property	Classical model	Experiment (*ab initio*)	Error in classical model
Phenol			
Density	0.86 g/cm^3	1.07 g/cm^3	20%
Dipole Moment	1.6 D	1.7 D (1.5 D)	7% (7%)
(parallel and perpendicular to CO bond)	1.6 D × 0.2 D	(1.4 D × 0.2 D)	(14% × 0%)
Phenylacetylene			
Density	1.03 g/cm^3	0.93 g/cm^3	11%
Dipole Moment	0.68 D	0.66 D	3%

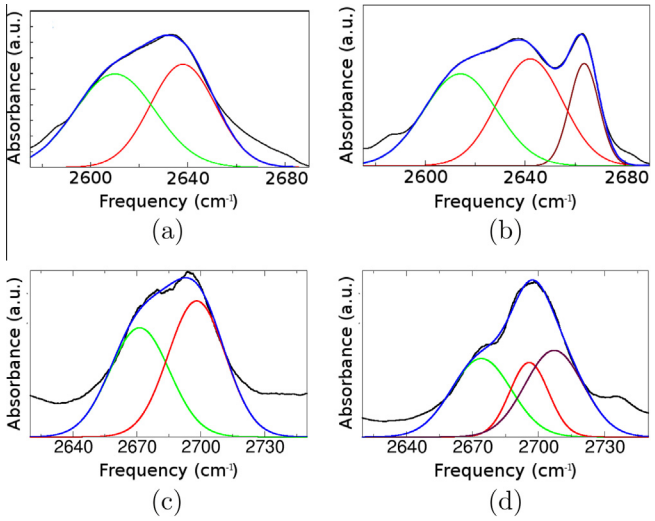

Fig. 4. Experimental IR spectrum for phenol in (a) pure phenylacetylene solvent and (b) carbon tetrachloride-diluted solvent. Simulated IR spectra of phenol in the (c) pure and (d) dilute solutions. The peaks correspond to triple-site binding (green), ring-site binding (red), and free vibration (mauve). The order and identity of the peaks from the MD simulations agree with experiment. Only the location of the free peak in the simulation deviates significantly from experiment, most likely due to the unmodified carbon tetrachloride MD potential.

the experimental time of ≈ 5 ps. For clarity, we have chosen (ω, ω') points corresponding to off-diagonal and diagonal peaks and plotted their intensity changes with time. These plots are given in Fig. 6, designated by their associated binding state and relative to the triple peak height. The agreement with experiment (where raw data are available) is very good. Most importantly, dilution with carbon tetrachloride does not seem to affect the rate of growth or decline of any of the peaks – a central fact used previously to argue that direct migration is the dominant mechanism. The larger difference in intensity between the two simulated curves in Fig. 6 is due to the overlap between the triple-site binding and free peaks in the IR and 2D-IR spectra of the solution diluted with carbon tetrachloride.

6. Statistical analysis of site migration

As seen above, the MD data produce IR and 2D-IR observables that are consistent with experiment. The 2D-IR is essentially a frequency-frequency correlation function, and frequency changes are used to identify the different local environments. However, with MD trajectory data in hand, it is possible to examine the local environment of the phenol OH directly and perform cross-correlations between binding states based on their spatial location[41]. Additionally, this allows one to distinguish between indirect and direct migration events.

Functions $f(t)_{T_i}$ are defined that are set equal to 1 when the phenol terminal hydrogen is closest to a carbon atom on the triple site of phenylacetylene i at time t and are set to 0 otherwise. Functions $f(t)_{R_j}$ are defined the same way but when the phenol terminal hydrogen is closest to a carbon atom on the ring site of phenylacetylene j at time t, with any residence times of less than 100 fs excluded (set to 0 for that interval). Due to the coarse nature of the criterion for binding set above, there are many cases in which the OH may briefly fluctuate outside the boundary of the binding zone of one site, which would be counted as a migration event, despite not fitting the physical intuition of one. Cross-correlating $f(t)_{T_i}$ with $f(t)_{R_j}$ for $i \neq j$ produces a curve that reveals the time scale of indirect migrations. Conversely, cross-correlating for $i = j$ produces a curve that reveals the time scale of direct migrations. As with the 2D-IR experiment, the cross-correlation only depends on the phenol binding state at the beginning and end of an interval of length τ; whether one or many migration events occur during this period is not reflected.

Such cross-correlations, averaged over all phenols and normalized for the finite time span of the MD runs, are shown in Fig. 7. The total site-site cross-correlation curve grows in on a similar time scale to the 2D-IR, indicating good agreement between the 2D-IR and binding site-binding site correlations. The direct and indirect cross-correlations each evince three time scales; attempts to fit the data to only two exponential functions yielded very poor results. The first one corresponds to fluctuations about the threshold of the hydration sphere around phenol of the kind discussed above, and can be described by an exponential with a characteristic time of about 230 fs for both pathways. A second process that corresponds to phenylacetylene molecules staying in the solvation sphere for a prolonged period of time before migrating has a characteristic time of about 4 ps. These first two time scales have been observed in similar MD studies as well [41]. Finally, a slower time scale can be identified with a characteristic time of about 30 ps for the indirect pathway, and 90 ps for the direct pathway. The nature of the process corresponding to this last time scale will be discussed below. In the dilute case, the intermediate and long time scales change only for direct migration, to 2 ps for the shorter and 60 ps for the longer.

These cross-correlations reveal that indirect migration is indeed favored in the highly dilute phenol in phenylacetylene solution (see Fig. 7). Dilution with carbon tetrachloride to the concentration reported brings the frequency of indirect migrations down to the point where direct migrations become the majority of events for the timespan from 0 to 5 ps, though overall indirect migrations are still more numerous. Importantly, the effect of CCl_4 dilution on the time scale of indirect migration is minimal. The site-site cross-correlation grows in on a time scale that is consistent with experimental observables for both the phenol in phenylacetylene solution and the CCl_4 diluted solution reported in the literature. However, despite this agreement indirect migration still remains the dominant pathway rather than direct migration. This is contrary to the conclusion presented in the experimental literature.

7. Quantum chemistry calculations of three-molecule complexes

To understand the conflicting conclusions from MD and experiment, the migration mechanisms were investigated in detail. Since dilute solutions of phenol in phenylacetylene are modeled in the current research, phenol–phenol interactions were not considered here. It was assumed that each phenol molecule can bind to one or more phenylacetylene molecules. The major intermolecular interaction types in this case include (a) hydrogen bonding between the hydrogen of a phenol OH and the triple or ring site of phenyl-

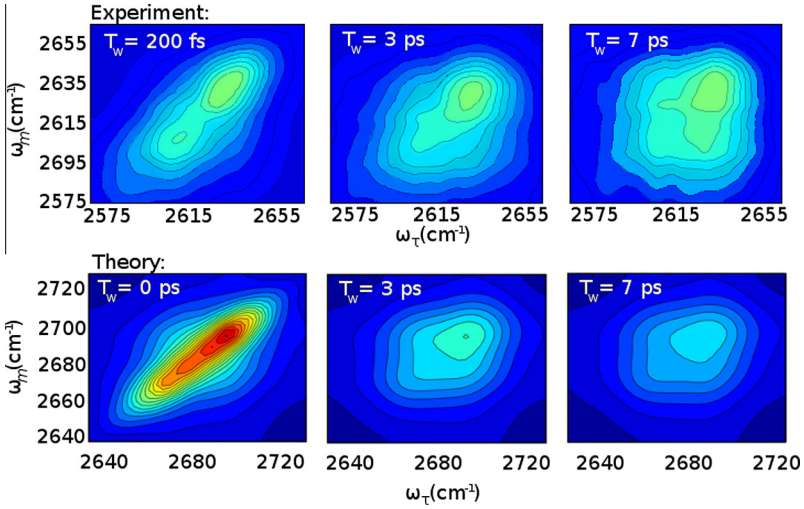

Fig. 5. Simulated and experimental 2D-IR spectra for phenol in solution of phenylacetylene. The simulated spectra were produced by interpolation of 4 ps long Fourier windows. The agreement between experiment and theory is good.

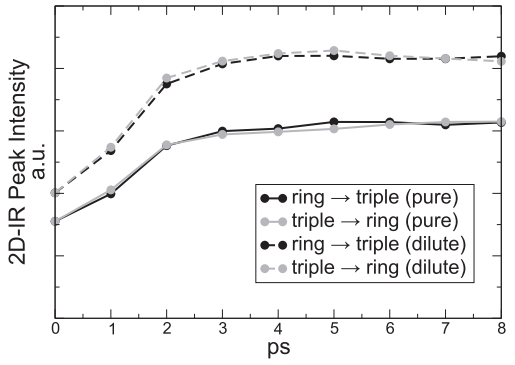

Fig. 6. 2D-IR peak heights relative to triple-site binding peak height as a function of time for the ring → triple off-diagonal peak and the triple → ring off-diagonal peak for both pure and dilute phenylacetylene solvent. As can be seen, dilution with carbon tetrachloride does not appreciably change the rate of peak growth.

acetylene, and (b) weaker phenyl-ring, or phenyl-triple site interactions. The latter can occur between CH hydrogen atoms and π-orbitals, or as π–π interactions.

Clusters formed by one phenol and two phenylacetylene molecules were investigated. As with the complexes formed by one phenol and one phenylacetylene, the structures obtained using the EFP method were chosen as initial points for geometry optimization with MP2 theory. Five complexes corresponding to energy minima at the MP2/6-31 + G (d,p) level are depicted in Fig. 8. The only three-molecule complex featuring hydrogen bonding to the ring site is 8(c). It has the lowest energy among all three-molecule complexes studied. The structure 8(e) shows hydrogen bonding between the hydroxyl group and only one phenylacetylene, and its interaction with the other phenylacetylene is pure π–π bonding.

Comparing the complexes in Fig. 8 one can see that all five have phenol hydrogen bonded to the triple bond of phenylacetylene, and all are stabilized by ring–ring bonding between the phenol and an adjacent phenylacetylene in a sandwich-like configuration. This suggests that phenol dynamics is primarily dictated by vdW forces, and the hydroxyl group of phenol forms a hydrogen bond with any proton acceptor available nearby.

The global minimum complex in Fig. 8(c) is found to have the hydroxyl primarily ring-site binding to one phenylacetylene and weakly triple-site binding to another. The complex next higher up in energy (8(b)) differs from 8(c) in that the phenol has shifted closer to the triple site of the adjacent phenylacetylene and now has a shorter hydrogen bond with the triple-site than with the ring-site. These two most stable complexes suggest that indirect migration can occur frequently because of phenol's preference to

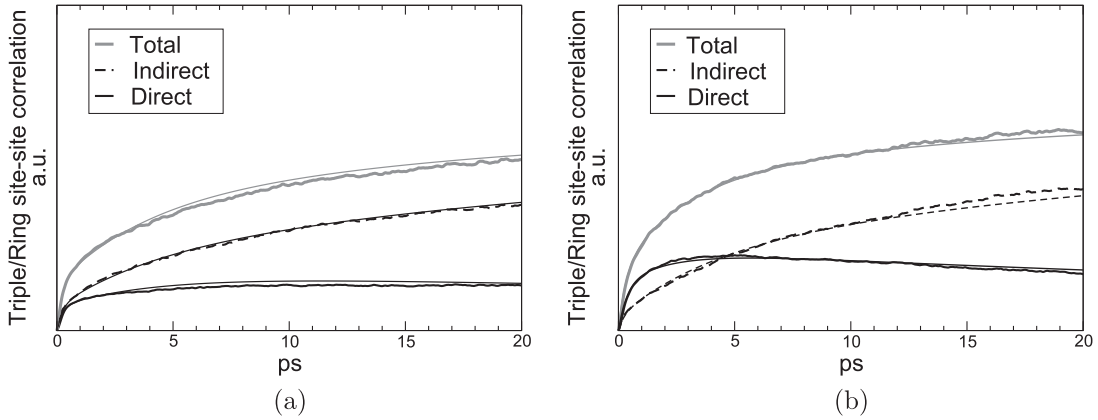

Fig. 7. Binding site-binding site cross-correlations corresponding to direct and indirect migration in the reference (a) highly-dilute phenol solution. The curves can each be fit (thin lines) to three exponentials with very fast, intermediate and long characteristic times. Dilution with carbon tetrachloride (b) sharply reduces the prevalence of indirect migration in the 0–5 ps range, while correlation with direct migration remained largely unchanged. The time scale of the growth does not differ significantly.

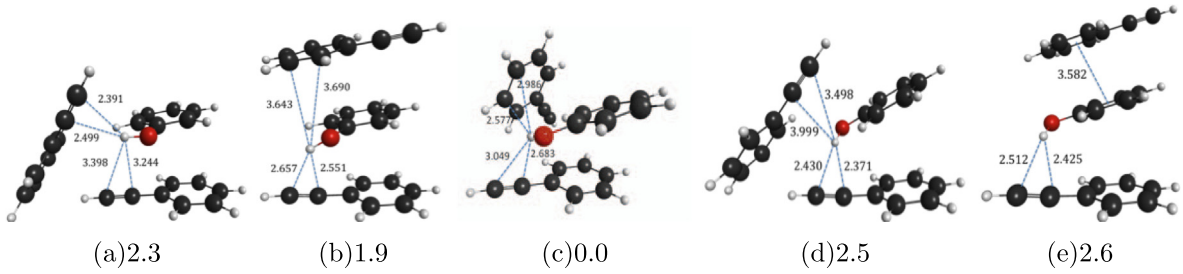

Fig. 8. MP2/6–31 G (d) optimized structures (distances in Å) and relative energies (in kcal/mol) of hydrogen-bonded complexes of phenol with two phenylacetylene molecules.

be sandwiched between two phenylacetylene triple- and ring-sites. In this configuration, it is quite easy for the phenol to rotate from the triple-site on one phenylacetylene to the ring-site on another. Phenol migration between two hydrogen bonding sites of the same phenylacetylene molecule (direct mechanism) can take place via sliding of a phenylacetylene molecule along a phenol-phenylacetylene pair. Since phenylacetylene is a conjugated system, this sliding occurs without breaking an OH-π bond at any time; i.e., with high rate. Therefore, the MP2 data qualitatively support both direct and indirect mechanisms of phenol migration between different hydrogen bonding sites in phenylacetylene solution.

8. Indirect migration pathway

The migration pathways were examined by analyzing the dynamics during identified migration events. Fig. 9 shows statistics for intermolecular distances and angles of a phenol and surrounding phenylacetylenes during migrations. During migrations of the kind shown in Fig. 9(a), the distance between the terminal phenol's oxygen and two binding sites on the nearest phenylacetylene are inversely related, with the interchange occurring rapidly at 1 ps, indicating that this migration is direct. We also find that the angle of the phenol to the nearest phenylacetylene stays between 40° and 90°, consistent with a T-complex geometry. Throughout the migration, the next-nearest phenylacetylene remains at a roughly constant distance, and we observe an angle with phenol $< 30°$, consistent with a stacking configuration. These data suggest that direct migrations occur with phenol in a T-complex that is stabilized by a second nearby phenylacetylene. The migration in Fig. 9(b) is markedly different. Here, the distances of phenol to triple- and ring-sites on different phenylacetylenes are inversely related, indicating an indirect migration. From the absolute distances to the origin ('A') and destination ('B') phenylacetylenes, it is clear that both are close throughout the migration, strongly supporting the notion of a three-molecule complex. However, the angles of the phenol with the phenylacetylenes participating in indirect migration do not rise above 20°; in contrast to direct migrations, all nearby phenylacetylenes prefer to be oriented in a "stacking" configuration. The data for both migrations are in good agreement with the *ab initio* three-molecule energy minima, revealing migration dynamics that are dominated by these configurations.

From this information, a picture of the mechanism for indirect migrations emerges, as well as a possible explanation for the 2D-IR and spatial correlation results. It is evident in both the foregoing quantum chemistry calculations and molecular dynamics simulations that phenol and phenylacetylene dynamics are dominated by stacking and vdW interactions with phenol in close proximity to multiple phenylacetylenes. If given the chance, phenol will preferentially form a loose sandwich structure in which it lies between adjacent phenylacetylenes.

Indirect migrations mainly occur when phenol is bound in a three-molecule complex with two phenylacetylenes. In the solution of pure phenylacetylene the phenol is essentially always in a three-molecule complex, but in the dilute limit two-molecule complexes and unbound phenol are likely as well. In this three-molecule complex, the phenol hydrogen is able to migrate to the other phenylacetylene with an ease that is comparable to a direct migration. This explains the reduction in indirect migrations occurring in the dilute case observed in the cross-correlation data: the

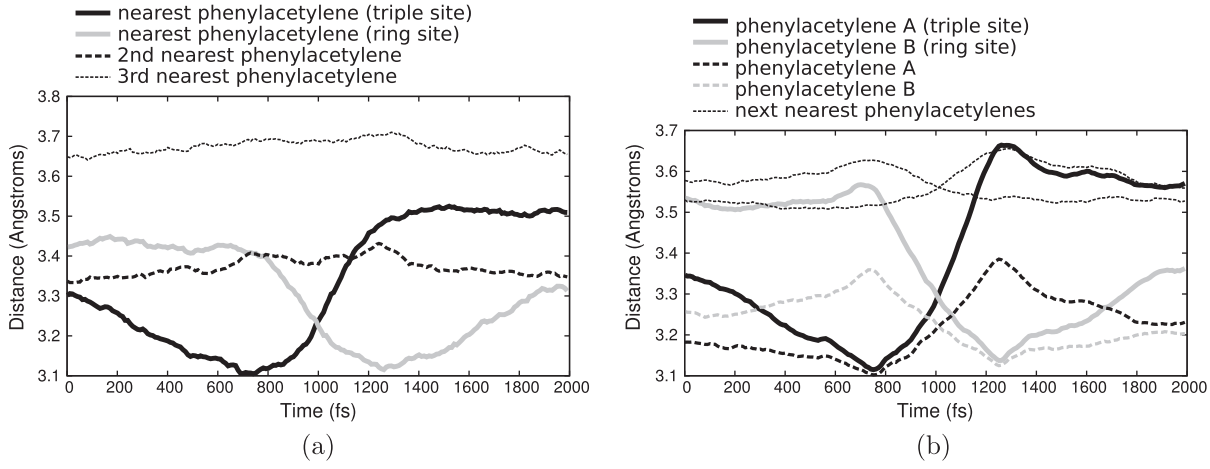

Fig. 9. Time evolution of the average distance between phenol and adjacent phenylacetylenes during (a) direct and (b) indirect triple → ring migration that occurs at the 1000 fs mark. Distances are from the terminal phenol's oxygen atom and the nearest carbon atom (or binding site, if indicated) of the phenylacetylene. In the direct case, a second phenylacetylene remains close throughout, appearing to mediate the exchange, and in the indirect case, the close proximity of both phenylacetylenes indicates a three-molecule complex of the kind characterized by the *ab initio* calculations.

frequency of indirect migrations is dependent on the population of three-molecule complexes, and the ratio of direct to indirect migrations reflects the presence of a significant number of two-molecule complexes in the dilute case. This also suggests that the longest time scale fit to the cross-correlation data, whose contribution is more prominent in the dilute case, corresponds to three-molecule complex formation which yields a slow rise in indirect migrations and breakup which results in a decay in direct migrations as phenols become permanently separated from the phenylacetylenes to which they were initially bound. Therefore the 2D-IR measurements, probing the < 10 ps time scale, only capture direct migrations and the indirect migrations in pre-existing three-molecule complexes. The formation (and breakup) of the three-molecule complexes will occur too slowly to appreciably affect the dynamics on the time scale observed by 2D-IR. Thus, the 2D-IR signal remains unchanged because the dominant indirect migrations proceed via first-order reaction dynamics and are as insensitive to phenylacetylene concentration as direct migration.

9. Conclusion

Experimental observations [18] of phenol dynamics in phenylacetylene were reproduced at a theoretical level using *ab initio* methods and classical molecular dynamics. It was demonstrated that classical dynamics is sufficient to treat the electrostatic and hydrogen bonding interactions between electrophiles and conjugated aromatic systems even when vdW forces are significant. Constructing a phenol potential with vibrational sensitivity to the local environment allowed for generation of a simulated 2D-IR spectrum directly from the dynamics that developed off-diagonal peak growth at a rate that agreed well with experiment for both pure and dilute phenylacetylene solvent.

Furthermore, quantum chemical studies revealed that the triple bond is the more favorable hydrogen binding site for the phenol hydroxyl when compared to the phenyl ring. Both EFP and MP2 methods show that a three-molecule sandwich stacking orientation is generally preferred in solution, due to increased π-π bonding. This is reflected in the dynamics, which indicates that migrations of the phenol hydroxyl between sites on different phenylacetylenes (indirect migration) are competitive with, or even preferred over intramolecular (direct) migrations. Crucially, in complexes with multiple phenylacetylene molecules, the hydroxyl hydrogen is easily able to migrate between molecules, resulting in the effective first order kinetics observed in 2D-IR.

Acknowledgments

L.K. was supported by the NSF under Grant No. CBET-1159736, S.M.Y was supported by the DOE under Grant No. DE-FG02-07ER46431, and A.M.R. was supported by the AFOSR under Grant No. FA9550-10-1-0248. M.S.G. and Y.K. were supported by the AFOSR Grant No. FA9550-08-1-0034. MDF thanks the NSF (Grant No. CHE-1157772) and the AFOSR (Grant No. FA9550-12-1-0050) for support. S.M.Y and A.M.R thank the HPCMO and NERSC for generous computational support. The authors also thank Daniel Rosenfeld for fruitful discussions on 2D-IR experiments.

Appendix A

The EFP potentials were used to locate stable phenol-phenylacetylene complexes. Four different structures, shown in Fig. 10, were located. Two structures (10(c), (d)) represent T-shaped hydrogen bonded complexes, and the other two (10(a), (b)) exhibit both π–π stacking and hydrogen bonding. With respect to the hydrogen bond position, two complexes (10(a), (d)) have the proton interacting with the triple site, while two others (10(b), (c)) are formed by hydrogen interaction with the ring site.

The relative energies of the four dimer complexes shown in Fig. 10 are all within ≈ 1.1 kcal/mol, with structure 10(a) predicted to be lowest in energy. All four structures along with a few more complexes from the MC run (that do not have corresponding min-

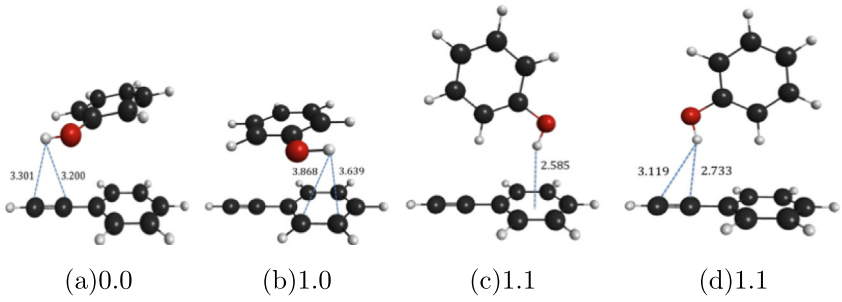

Fig. 10. Structures (distances in Å) and relative energies (in kcal/mol) of EFP optimized phenol-phenylacetylene complexes.

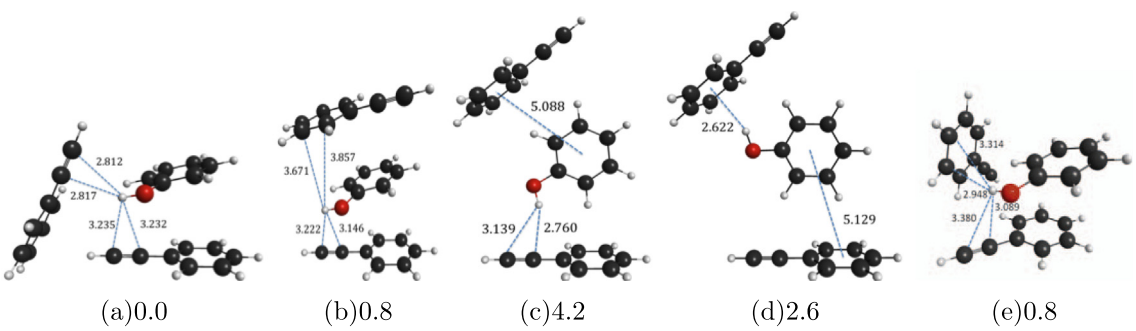

Fig. 11. EFP optimized structures (distances in Å) and relative energies (in kcal/mol) of H-bound complexes of phenol with two phenylacetylene molecules.

ima at the EFP level) were used for further computations using MP2.

Appendix B

Five minimum-energy structures of phenol complexes with two phenylacetylene molecules were located based on the initial low-energy geometries obtained with the MC/SA procedure, as well as by sampling the phase space using the MD potentials parametrized from the two-molecule MP2 results.

As seen in Fig. 11, the obtained three-molecule complexes can be classified into two groups: featuring triple-site H-bonding only (11(a)–(c)) and those having the hydroxyl proton bound to the ring-site of one of phenylacetylene molecules (11(d) and (e)). The global minimum 11(a) has two H-bonds with the triple sites of both phenylacetylenes. The low-energy structures 11(a), (b) and (d) involve π-π stacking, while the complexes without π-π bonding (11(c) and (d)) are higher in energy.

Interestingly, all five structures contain sub-structures that are similar to the dimer species described above. For example, structures 11(a) and (e) resemble a second phenylacetylene molecule bound to the EFP complex 10(a); structure 11(b) has some similarity with structures 10(a) and (b); structure 11(c) consists of a T-shaped complex with some similarity to 10(d); and structure 11(d) has a phenol hydrogen pointing to the center of a phenyl ring of phenylacetylene, like structure 10(c).

References

[1] B.O. Haglund, R. Joshi, K.J. Himmelstein, Journal of controlled release 41 (1996) 229.
[2] M. Armand, F. Endres, D.R. MacFarlane, H. Ohno, B. Scrosati, Nature materials 8 (2009) 621.
[3] M.L. Waters, Current opinion in chemical biology 6 (2002) 736.
[4] Z. Chen, A. Lohr, C.R. Saha-Möller, F. Würthner, Chemical Society Reviews 38 (2009) 564.
[5] G.C. Pimentel, A. McClellan, Annual Review of Physical Chemistry 22 (1971) 347.
[6] G.C. Pimentel, A.L. McClellan, The Hydrogen Bond, Freeman, WH, 1960.
[7] G.A. Jeffrey, G.A. Jeffrey, An Introduction to Hydrogen Bonding, vol. 12, Oxford University Press New York, 1997.
[8] H. Graener, T.Q. Ye, A. Laubereau, Journal of Chemical Physics 90 (1989) 3413.
[9] S. Suzuki, P. Green, R. Bumgarner, S. Dasgupta, W. Goddard, G. Blake 257 (1992) 942–945.
[10] K. Liu, J. Cruzan, R. Saykally, Science 271 (1996) 929.
[11] A. Luzar, D. Chandler, Nature 379 (1996) 55.
[12] H.J. Bakker, S. Woutersen, H.K. Nienhuys, Chemical Physics 258 (2000) 233.
[13] B. Chen, I. Ivanov, M.L. Klein, M. Parrinello, Physical Review Letters 91 (2003) 215503.
[14] C.J. Fecko, J.D. Eaves, J.J. Loparo, A. Tokmakoff, P.L. Geissler, Science 301 (2003) 1698.
[15] M.L. Cowan, B.D. Bruner, N. Huse, J.R. Dwyer, B. Chugh, E.T.J. Nibbering, T. Elsaesser, R.J.D. Miller, Nature 434 (2005) 199.
[16] J.B. Asbury, T. Steinel, C. Stromberg, S.A. Corcelli, C.P. Lawrence, J.L. Skinner, M.D. Fayer, Journal of Physical Chemistry A 108 (2004) 1107.
[17] J.D. Eaves, J.J. Loparo, C.J. Fecko, S.T. Roberts, A. Tokmakoff, P.L. Geissler, Proceedings of the National Academy of Sciences of the United States of America 102 (2005) 13019.
[18] D.E. Rosenfeld, K. Kwak, Z. Gengeliczki, M.D. Fayer, Journal of Physical Chemistry B 114 (2010) 2383.
[19] R. Sedlak, P. Hobza, G.N. Patwari, Journal of Physical Chemistry A 113 (2009) 6620.
[20] P.C. Singh, B. Bandyopadhyay, G.N. Patwari, Journal of Physical Chemistry A 112 (2008) 3360.
[21] A. Sapse, D. Jain, International Journal of Quantum Chemistry 33 (1988) 69.
[22] K. Hasegawa, T. Masuda, T. Higashimura, Macromolecules 8 (1975) 255.
[23] M. Khalil, N. Demirdoven, A. Tokmakoff, Journal of Chemical Physics 121 (2004) 362.
[24] Y. Kim, R. Hochstrasser, Journal of Physical Chemistry B 110 (2006) 8531.
[25] M. Asplund, M. Lim, R. Hochstrasser, Chemical Physics Letters 323 (2000) 269.
[26] S. Park, K. Kwak, M.D. Fayer, Laser Physics Letters 4 (2007) 704.
[27] J.R. Zheng, K. Kwac, J. Asbury, X. Chen, I.R. Piletic, M.D. Fayer, Science 309 (2005).
[28] J. Zheng, K. Kwak, M.D. Fayer, Accounts of Chemical Research 40 (2007) 75.
[29] M.W. Schmidt, K.K. Baldridge, J. Boatz, S.T. Elbert, M.S. Gordon, J.H. Jensen, S. Koseki, N. Matsunaga, K.A. Nguyen, S.J. Su, T.L. Windus, M. Dupuis, J.A. Montgomery, Journal of Computational Chemistry 14 (1993) 1347.
[30] M.S. Gordon, M.A. Freitag, P. Bandyopadhyay, J.H. Jensen, V. Kairys, W.J. Stevens, Journal of Physical Chemistry A 105 (2001) 293.
[31] I. Adamovic, M.S. Gordon, Journal of Physical Chemistry A 110 (2006) 10267.
[32] T. Smith, L.V. Slipchenko, M.S. Gordon, Journal of Physical Chemistry A 112 (2008) 5286.
[33] K. Kwak, J. Zheng, H. Cang, M.D. Fayer, Journal of Physical Chemistry B 110 (2006) 19998.
[34] C. Mller, M.S. Plesset, Physical Review 46 (1934) 618.
[35] C.M. Aikens, S.P. Webb, R.L. Bell, G.D. Fletcher, M.W. Schmidt, M.S. Gordon, Theoretical Chemistry Accounts 110 (2003) 233.
[36] S. Liu, S. Srinivasan, M.C. Grady, M. Soroush, A.M. Rappe, The Journal of Physical Chemistry A 116 (2012) 5337–5348. <http://pubs.acs.org/doi/pdf/10.1021/jp2124394>.
[37] J. Wang, R. Wolf, J. Caldwell, P. Kollman, D. Case, Journal of Computational Chemistry 25 (2004) 1157.
[38] K. Kwac, C. Lee, Y. Jung, J. Han, K. Kwak, J. Zheng, M.D. Fayer, M. Cho, Journal of Chemical Physics 125 (2006), http://dx.doi.org/10.1063/1.2403132.
[39] S.J. Plimpton, Journal of Computational Physics 117 (1995) 1.
[40] S. Melchionna, G. Ciccotti, B. Holian, Molecular Physics 78 (1993) 533.
[41] V.A. Makarov, B.K. Andrews, P.E. Smith, B.M. Pettitt, Biophysical Journal 79 (2000) 2966.